A Regional Characterization and Assessment of Geologic Carbon Sequestration Opportunities in the Upper Cambrian Mount Simon Sandstone in the Midwest Region

MRCSP Phase II Topical Report
October 2005–October 2010

Authors

Cristian Medina,[1] John Rupp,[1] Katharine Lee Avary,[2] Eric R. Venteris,[3] David A. Barnes,[4] John A. Harper,[5] Steve Greb,[6] Brian E. Slater,[7] Alexa Stolorow,[7] and Joel Sminchak[8]

[1]Indiana Geological Survey
[2]West Virginia Geological and Economic Survey
[3]Ohio Division of Geological Survey
[4]Western Michigan University
[5]Pennsylvania Geological Survey
[6]Kentucky Geological Survey
[7]New York State Museum
[8]Battelle Memorial Institute

DOE Cooperative Agreement No. DE-FC26-05NT42589
OCDO Grant Agreement No. DC-05-13

NOTICE

A Regional Geologic Characterization and Assessment of Geologic Carbon Sequestration Opportunities in the Upper Cambrian Mount Simon Sandstone in the Midwest Region

Midwest Regional Carbon Sequestration Partnership (MRCSP)
Phase II Task Report Period of performance: October 2005 – October 2010

Authors

Cristian Medina[1], John Rupp[1], Katharine Lee Avary[2], Eric Venteris[3], Dave Barnes[4], John Harper[5], Steve Greb[6], Brian Slater[7], Alexa Stolorow[7], Joel Sminchak[8].

1 Indiana Geological Survey
2 West Virginia Geological and Economic Survey
3 Ohio Division of Geological Survey
4 Western Michigan University
5 Pennsylvania Geological Survey
6 Kentucky Geological Survey
7 New York State Museum
8 Battelle Memorial Institute

ABSTRACT

The Upper Cambrian Mount Simon Sandstone is recognized as a deep saline reservoir that has significant potential for geological sequestration in the Midwestern region of the United States. Porosity and permeability values collected from core analyses in rocks from this formation and its lateral equivalents in Indiana, Kentucky, Michigan, and Ohio indicate a predictable relationship with depth owing to diagenetic changes in the pore structure. This predictive relationship is useful for evaluating the geological carbon sequestration capacity in the Midwestern region. Porosity logs from wells in the study area provide additional sources of petrophysical data. The regional trend of decreasing porosity with depth is described by the equation: $\varphi\,(d) = 16.36 * e^{-0.00012*d}$, where φ equals porosity and d is depth in feet. The correlation between burial depth and porosity can help predict the petrophysical character of the Mount Simon Sandstone in more deeply buried and largely undrilled portions of the basins. Understanding the relationships among porosity, permeability and depth also provides information for use in numerical models that simulate supercritical carbon dioxide flow within the Mount Simon Sandstone. The decrease of porosity and permeability with depth generally holds true on a basinwide scale. However, localized stratigraphic and spatial variations in sedimentary facies within the sequence can also affect reservoir quality. In fact, a reversal in this trend of decreasing porosity with depth has been observed in some areas. Careful documentation of the mineralogical and sedimentological characteristics of the reservoir is critical to the successful prediction of the petrophysical attributes of deep saline aquifer systems and how they will perform at a given locality as a sequestration reservoir for carbon dioxide. In spite of the three-dimensional variation in lithologic and petrophysical character within the Mount Simon Sandstone, we used the source data that helped us to predict porosity to estimate the pore space in the reservoir that may serve for geological sequestration of CO_2. The storage capacity estimated for the Mount Simon Sandstone in the western part of the MRCSP region, using efficiency factors of 1%, 5%, 10%, and 15% respectively, is 23,680, 118,418, 236,832, and 355,242 [MM Tons CO_2], respectively.

CONTENTS

LIST OF FIGURES AND TABLES

ACRONYMS USED IN THIS REPORT

CCS – carbon capture and storage

CO_2 – carbon dioxide

DOE – Department of Energy

DEM – digital elevation model

GR – gamma-ray

GSC – Geological Sequestration Capacity

MRCSP – Midwest Regional Carbon Sequestration Partnership

NETL – National Energy Technology Laboratory

UIC – Underground Injection Control

UNIT ABBREVIATIONS USED IN THIS REPORT

API – oil gravity

°C – degrees Celsius

°F – degrees Fahrenheit

ft – foot

ft^2 – square feet

ft^3 – cubic feet

g/cc – grams per cubic centimeter

km – kilometer

lb – pound

m – meter

md – millidarcy

m^3 – cubic meter

MMt – million metric tones

MPa – megapascal

psi – pounds per square inch

µd– microdarcy

1. INTRODUCTION

Geological Sequestration of anthropogenic carbon dioxide (CO_2) from stationary emissions sources is an important component of the greenhouse gas emissions reduction strategy termed carbon capture and storage (CCS). The feasibility of cost-effective geological sequestration in any area is fundamentally dependant on local and suitable geological sequestration systems, including effective reservoir zones for injection and storage and stratigraphically related seals for confinement. The geological sequestration system must lie at a depth within the subsurface sufficient to retain CO_2 in supercritical state (Figure 1 and 3), possess sufficient injectivity and storage capacity for the scale of the project under consideration, and have injection and confining zone characteristics that preclude buoyant, supercritical CO_2 escape over long periods of time (generally accepted to exceed at least 1,000 years, see IPCC, 2005 for details). National and international research programs have been undertaken in recent years (e.g. the Department of Energy/National Energy Technology Laboratory, Regional Carbon Sequestration Partnership Program, DOE/NETL, 2008) to evaluate CO_2 sources and sinks including the evaluation of regional storage capacity of significant geological sequestration targets. As a result, the Midwest Regional Carbon Sequestration Partnership (MRCSP) was formed to assess the geology of the Midwest and some selected eastern states of the United States for their potential to store large volumes of injected CO_2 in the deep subsurface.

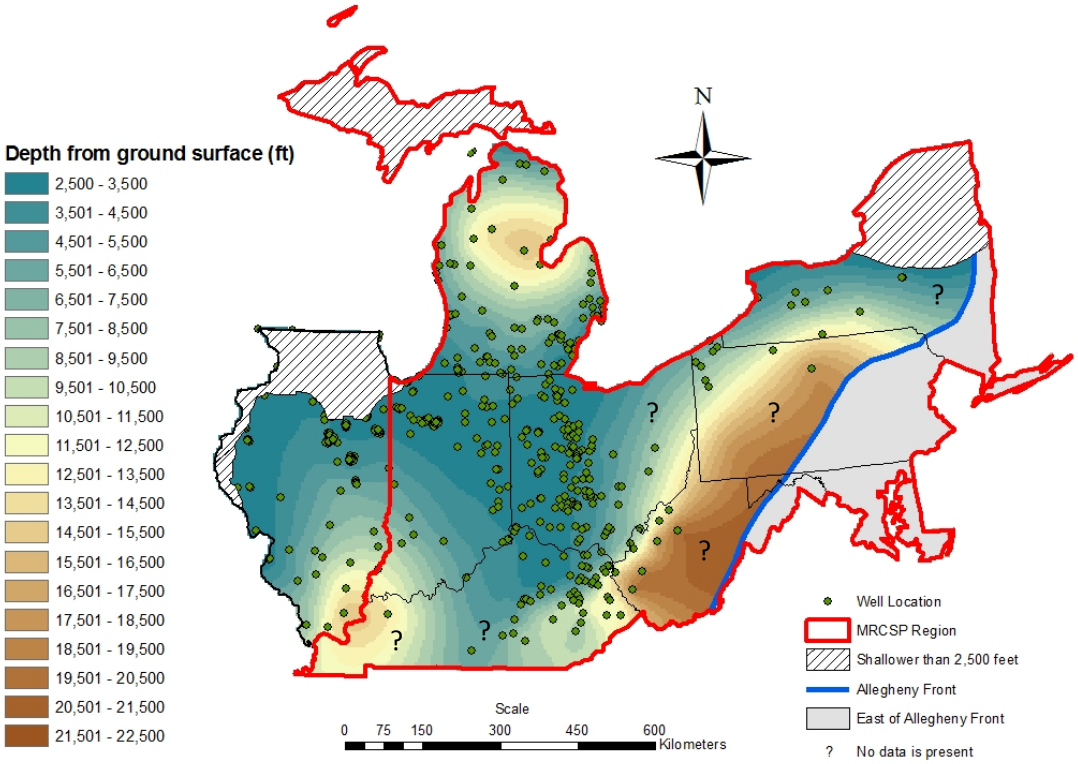

Figure 1. Depth to the top of the Mount Simon Sandstone and other basal sandstones obtained from interpolation of data from 1,047 wells. Illinois is included here even though it is not part of the MRCSP region to give a better perspective of the Illinois Basin configuration. Question marks denote higher uncertainty associated with absence of well data.

A prime target identified in the Midwest region is the Upper Cambrian Mount Simon Sandstone (Figure 2), a term that refers to parts of the "basal sand" as mapped by the MRCSP (Wickstrom et al., 2005). The basal sand in much of the western part of the MRCSP study area shown in Figure 1 is equivalent to the Mount Simon, but the Mount Simon pinches out to the south and east, and other, sometimes older Cambrian sandstone constitute the basal sand at those localities.

The Mount Simon has served as an important reservoir for many Class I Underground Injection Control (UIC) wells in several of the MRCSP states for many decades. The Mount Simon also serves as a significant gas storage reservoir in areas of the Illinois basin. Geological Sequestration Capacity (GSC) for all the Cambrian age basal sandstones in the Midwest (Indiana, Kentucky, Michigan, and Ohio) has recently been estimated to range from 50 to nearly 200 billion metric tons (DOE/NETL, 2008).

The Cambrian Mount Simon Sandstone unconformably overlies Precambrian igneous and metamorphic basement in much of the Illinois and Michigan basins, or Precambrian sediments of the Middle Run Formation in parts of the Illinois basin, and across parts of the Arches province. In much of eastern Ohio and other parts of the region it overlies metamorphic rocks of the Greenville complex. In the central Appalachian basin, the Mount Simon is likely equivalent to sandstones in the Maryville Formation of the Conasauga Group (Hickman and Harris, 2004; Harris et al., 2004). Deeper and older sandstones occur within the Rome Formation in the Rome Trough of Kentucky and West Virginia. Likewise, deep sandstones in the Rough Creek graben, in the southern part of the Illinois basin in western Kentucky, are likely older than the Mount Simon and overlie Precambrian basement in the graben. The Potsdam Sandstone of eastern Ohio, Pennsylvania, and New York unconformably overlies igneous and metamorphic Precambrian basement rocks in the northern Appalachian Basin.

The Mount Simon Sandstone is overlain conformably by the Eau Claire Formation (Cambrian) and its lateral equivalents in the Illinois and Michigan basins, and across the arches province. Deeper sandstones in the Rome Formation in the Rome Trough are overlain by shales of the Rome Formation, or shales, carbonates, and sandstones of the Conasauga Group. The Potsdam Sandstone is overlain by the dolomites and sandstones of the Galway Formation. Characteristics of these overlying units are discussed in the MRCSP Phase I report (Wickstrom et al., 2005).

In the Illinois and Michigan basins, the Mount Simon Sandstone is described as white, pink or purple, well rounded to angular, fine- to coarse- grained, poorly to moderately sorted, and arkose to quartz arenite (Driese et al., 1981; Makowitz and Milliken, 2003; Makowitz et al., 2006). Cements include quartz and feldspar overgrowths, hematite and calcite as replacement cements, and less frequently kaolinite, chlorite, and microquartz (Hoholick et al., 1984). Glauconite is a common constituent of the unit.

The depth of the Mount Simon Sandstone (and its equivalents or older Cambrian sandstones) is variable across the region, and ranges from less than 800 m (2,500 ft) in northwest Indiana and western Ohio along the Kankakee Arch to more than 6,000 m (20,000 ft) in the deeper parts of the basins (Figure 1). The origin of the clastic material that constitutes the Mount

Simon are sediments sourced in the Precambrian Shield and associated with the Wisconsin Arch (Makowitz and Milliken, 2003). These sediments are transgressive in nature and were deposited mostly in a marine embayment (Driese et al., 1981; Hoholick et al., 1984; Willman et al., 1975).

In order to ensure that the CO_2 injected into deep saline aquifers is in the supercritical phase (and significantly more dense than the gaseous phase), the pressure and temperature within the reservoir must be at least 7.4 MPa (1,073 psi) and 31^{o}C (87.8 ^{o}F) (above the critical point of CO_2). At surface conditions (25 ^{o}C; 77 ^{o}F and 0.1 MPa; 14.5 psi), CO_2 behaves as a gas with a density of 1.8 kg/m3 (0.11 lb/ft^3). A phase diagram of CO_2 shows the pressure and temperature conditions at which CO_2 behaves as a supercritical phase (Figure 3). Assuming normal geothermal and pressure gradients of 30 ^{o}C/ and 10.5 MPa/km (0.026 ^{o}F/ft and 0.43 psi/ft), respectively, it is then inferred that CO_2 can be stored as a supercritical fluid at depths in excess of 800 m (~2,500 ft). This minimum threshold value corresponds to a density of CO_2 no less than 260 kg/m^3 (16.23 lb/ft^3) (Lemmon et al., 2008), and as the density of the CO_2 increases with pressure, greater quantities of CO_2 could potentially be stored within the same pore volume in deeper aquifers. Increasing the CO_2 density also increases the storage safety because the buoyancy forces that drive upward migration decrease in heavier fluids (Solomon, 2006). The top of the Mount Simon Sandstone, therefore, must occur at depths greater than 800 m (2,500 ft) for it to be a suitable carbon sequestration target in the region.

The thickness of the Mount Simon ranges from less than 15 m (50 ft) in central Ohio on the western flank of the Appalachian basin to more than 600 m (2,000 ft) as it approaches the depocenter in the northern part of the Illinois basin (Figure 5). It appears to pinch out in western Kentucky mostly north of the Rough Creek fault zone. It also thins and pinches out into the Rome Trough of the Appalachian basin. In both areas, there are locally deeper and older sandstones which are included with the Mount Simon thickness map shown as Figure 5.

Regional analyses of available Mount Simon data confirm and expand upon the relationship between porosity and depth previously determined by Hoholick et al. (1984). This relationship is characteristic for the Mount Simon in the MGSC and MRCSP regions, and can be used to predict porosity when details about the petrophysical properties of the subsurface are unknown. The distribution of the sandstone, however, is variable, and most of the thick sections of the unit from which the relationship is partly based, are present only in Illinois, Indiana, and Michigan. A significant facies change is observed in central Ohio, east of which the basal sand becomes more argillaceous and thin. In portions of Kentucky and West Virginia, the Mount Simon pinches out and an older basal sand fills the Rome Trough (Ammerman and Keller, 1979; Shrake, 1991; Shrake et al., 1991), and possibly the Rough Creek Graben. These deeper sandstones appear to be restricted to a narrow band of graben-filling structures but they are still included in the Mount Simon porosity/depth relationship. Within the deep portion of the Appalachian basin, the extent and character of the basal sand is generally unknown. The Potsdam Sandstone of New York may have lateral equivalents in northwestern Pennsylvania and northern West Virginia (Ryder, 1991). The bulk of the data points and the relationship that is described herein apply to the Mount Simon Sandstone in the eastern and western portions of the MGSC and MRCSP regions, respectively (Figure 2).

This report presents the results of a more refined regional assessment of Mount Simon Sandstone GSC in the Midwestern region based on conventional core and wire-line log data analysis.

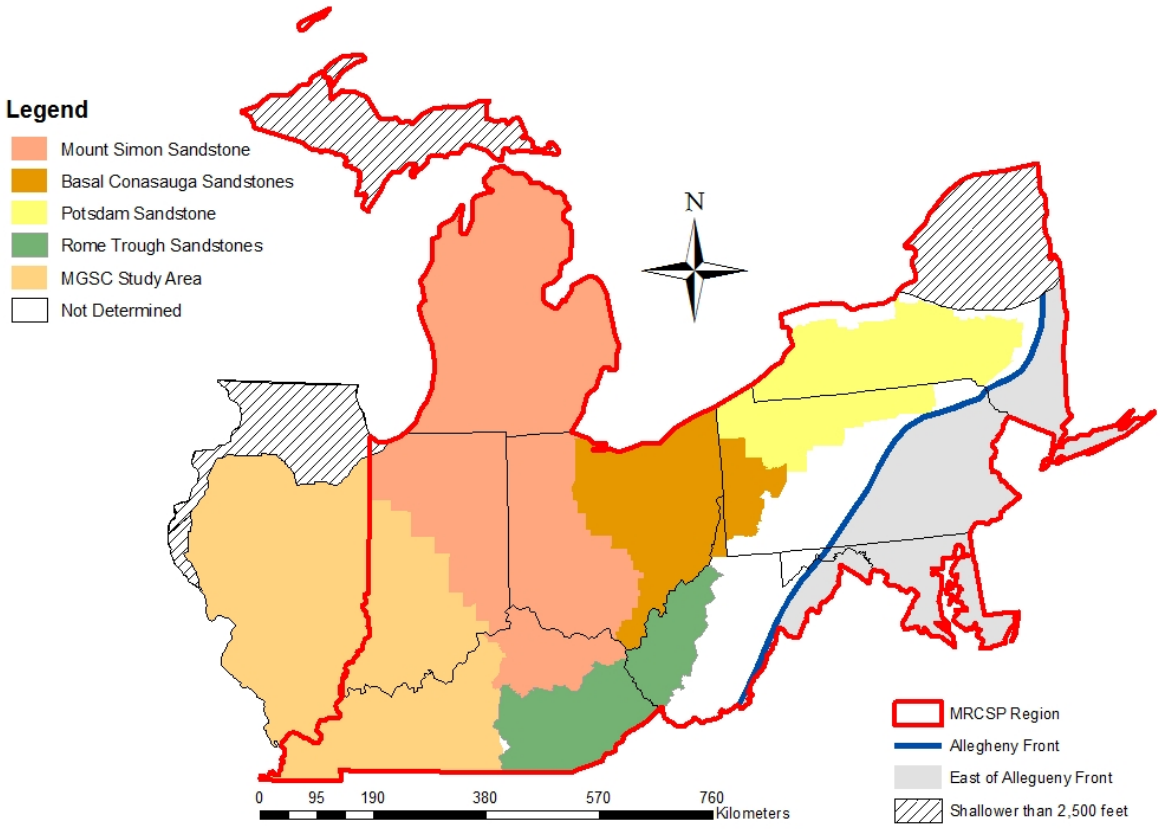

Figure 2. MRCSP Cambrian basal sandstone distribution.

2. GEOLOGY AND STRATIGRAPHY

The Mount Simon Sandstone in the Midwest region is characterized by predominantly quartzose sandstone with minor amounts of shale and dolomite that was first described in outcrop in Wisconsin by Ulrich (in Walcott, 1914, p. 354). The unit is in most places a quartz arenite but in some localities the lower portion of the unit becomes arkosic with significant amounts of glauconite, orthoclase feldspar and detrital mica. The Mount Simon constitutes the basal, transgressive sandstone unit of the Sauk sequence (Sloss, 1963) that unconformably overlies various Pre-Cambrian rock types in the Midwest from western Ohio to the proto Michigan-Illinois basin in Illinois, Indiana, western Kentucky, and Michigan (Figure 4) (Baranoski, 2007; see also, Wickstrom, et. al., 2005, for a lengthy discussion of early work and regional stratigraphy).

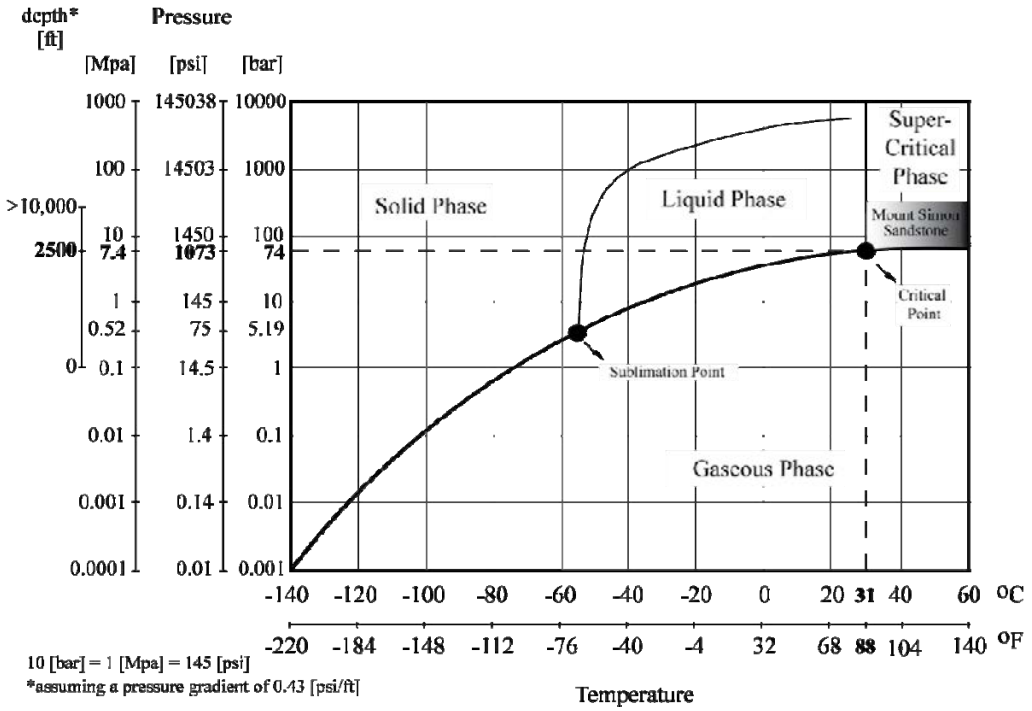

Figure 3. Phase diagram of CO_2. The diagram also displays the pressure and temperature conditions for the samples used in this study.

The Mount Simon Sandstone reaches a maximum thickness of nearly 2,500 ft (762 m) in the northeastern Illinois Basin (Figure 5) and is overlain by the Eau Claire Formation throughout the Midwest (Willman, et. al., 1975; Wickstrom et. al., 2003). The Eau Claire consists of low porosity crystalline dolomite, sandy dolomite, dolomitic and feldspathic sandstone, siltstone and shale and, along with overlying upper Cambrian strata, is identified as a regional confining zone in the Midwest (Wickstrom et. al., 2005).

The isopach map of the Mount Simon is not concordant with thickness maps of younger units found in the Michigan and Illinois basins. This discordance indicates the existence of a different depocenter and paleogeography for the early Paleozoic sediments when contrasted with younger deposits, and are not directly related to subsequent Paleozoic subsidence patterns in the basins (Howell and van der Pluijm, 1999). This isopach map (Figure 5) for the Mount Simon Sandstone was based on data interpreted from wire-line log data and drillers' logs, when available. The base of the Mount Simon is identified by a substantial increase in gamma-ray (GR) log signature above 50 to 100 API units, although many Mount Simon wells in Michigan have questionable log data (Barnes et al., 2009). In most well the top of the Mount Simon is identified by a decrease in the GR log signature consistently to less than 50 API units. The overlying Eau Claire Formation generally displays a gamma ray signature of greater than 75 API units. These log criteria are spatially variable, however, due to inferred facies changes throughout the region.

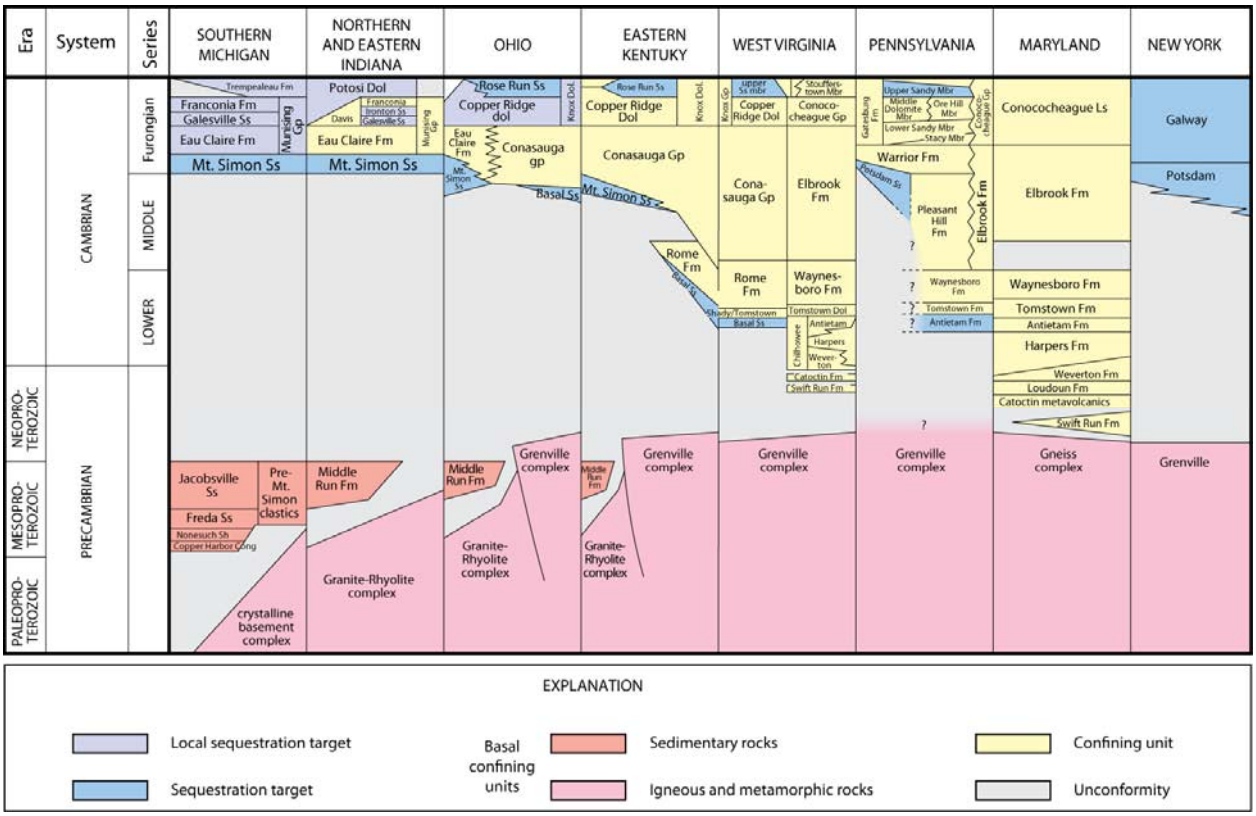

Figure 4. Regional stratigraphic correlation chart for the Cambrian and Precambrian periods indicating CO_2 sequestration targets and confining units within the MRCSP region.

3. METHODOLOGY

3.1 CORE ANALYSES AND GEOPHYSICAL LOGS TO POROSITY

Well data consisting of core analyses and geophysical logs were compiled and processed to derive the porosity-depth relationships that show the changes in porosity due to diagenetic processes. Log-derived porosity values were obtained from sonic, density, and neutron porosity logs (Table 1). The formulas applied were (Asquith and Krygowski, 2004):

$$\emptyset_{sonic} = \frac{\Delta t_{log} - \Delta t_{ma}}{\Delta t_f - \Delta t_{ma}} \qquad [1]$$

where $\emptyset_{sonic}$ = sonic-derived porosity; Δt_{ma} = interval transit time of the matrix = 47.6 [µs/ft] in limestone (Schlumberger, 1972); Δt_{log} = interval transit time of formation; and Δt_f = interval transit time of the fluid in the well bore (fresh mud = 189 µs/ft). Similarly, porosity values were estimated using density logs:

$$\emptyset_{den} = \frac{\rho_{ma} - \rho_b}{\rho_{ma} - \rho_f} \qquad [2]$$

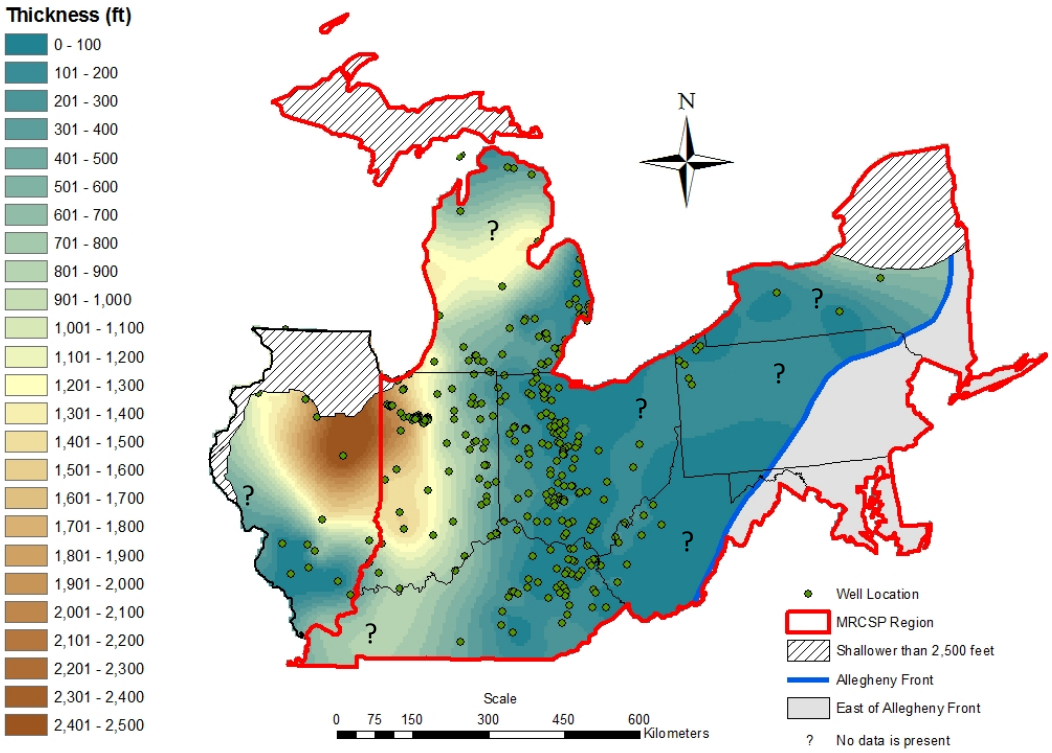

Figure 5. Gross isopach map obtained from the interpolation of 391 wells from the Mount Simon Sandstone and other basal sandstones in the study area (MRCSP region and Illinois). Question marks denote higher uncertainty associated with absence of well data.

where φ_{den} = density-derived porosity; ρ_b = formation bulk density; ρ_{ma} = matrix density = 2.71 [g/cc] in limestone (Schlumberger, 1972); and ρ_f = fluid density (1.1 in salt mud, 1.0 in fresh mud (used here), and 0.7 in gas, in g/cc).

Porosity values derived from neutron porosity logs were adjusted to reflect the fact that the log was run in a limestone matrix. Consequently, a linear transformation was applied by adding a decimal value of 0.04 to the original value of the neutron log curve to account for the change in matrix value (see Asquith and Krygowski, 2004, p. 42).

Table 1. Number of wells, by state, with core analyses and geophysical logs. These data are displayed in Figure 7.

		Geophysical Logs		
	Core Analyses	Neutron	Sonic	Density
Indiana	25	17	11	4
Kentucky	1	36	22	40
Michigan	11	22	10	36
Ohio	3	32	21	31
Total	40	107	64	111

When more than one type of porosity log was present, we determined the value of porosity as the arithmetic average between the available logs. Porosity data from core analyses were also used to calibrate the geophysical logs by running a linear regression of the values of porosity from the geophysical logs and the values from the core analyses taken at each well. The calibration then modified the values of log-derived porosity so that the regression equation followed a 1:1 relationship (Figure 6). This approach has the advantage of providing porosity values that are calibrated to realistic values taken from core analyses. A similar approach was also applied to sandstone from an oil recovery project in New Mexico (Martin et al., 1999).

Understanding the role that burial depth may play in changing the porosity of the sandstone fabric will allow a more realistic assessment of the total pore volume that is potentially available for the storage of supercritical CO_2. However, porosity from core analyses only represents a fraction of the vertical stratigraphic sequence. Therefore, average values of porosity, when combined with data from digital log curves, are needed to understand and predict regional trends and changes in porosity with depth.

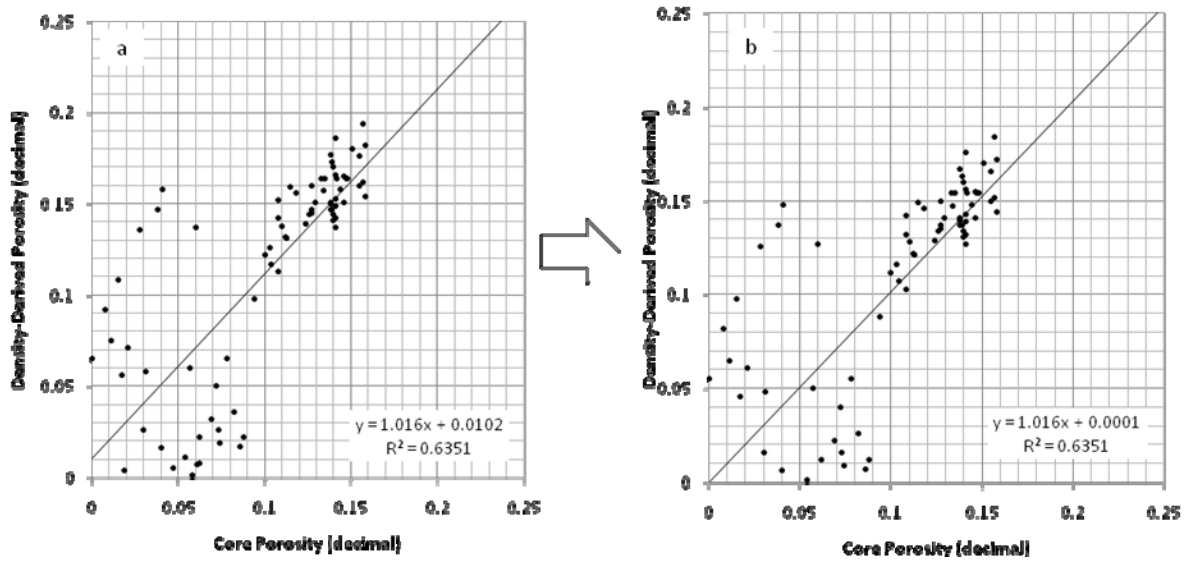

Figure 6. An example of geophysical log calibration using core data. Log-derived porosity is corrected (a) so that the linear regression between core and log-derived data follows a 1:1 relationship (b).

4. RESULTS

4.1 VARIATION IN MOUNT SIMON SANDSTONE RESERVOIR QUALITY WITH DEPTH

Porosity values derived from geophysical logs and porosity values from core analyses were plotted with depth (Figure 7). Core analyses consisted in 3,722 samples taken from 25 wells in Indiana (2,995 data points), 11 wells in Michigan (492 data points), 3 wells in Ohio (222 data points), and 1 well in Kentucky (13 data points). The exponential regression obtained from a simple regression run in Excel 2007, indicates that porosity decreases with burial depth. These two variables are related by the equation:

$$Ø(d) = 16.36 * e^{-0.00012 * d} \quad r^2 = 0.41 \qquad [3]$$

where Ø equals porosity (percent) and d is depth in feet.

This equation suggests that at a depth of 7,000 ft from the surface, porosity is reduced to approximately 7 percent (Figure 7). Below this depth the amount of porosity decreases exponentially and therefore the capacity of the reservoir does as well. These values are reasonable thresholds for maximum depth and minimum porosity and can be used for estimating the potential CO_2 storage volume in the Mount Simon Sandstone.

Other workers have recognized the depth dependence of porosity and reservoir quality in the Mount Simon Sandstone in the Midwest. Hoholick, et. al. (1984) presented careful documentation of diagenetic trends relative to burial depth in the Mount Simon in the Illinois basin and interpreted the increase in quartz overgrowth cements with depth as a main porosity reducing mechanism. That study indicated substantial reductions in porosity below 7,000 ft.

Medina et al. (2008) documented the relationship of reduction in porosity and permeability with depth for the area of the MRCSP. A global trend of increasing quartz overgrowth cementation and porosity occlusion with depth due to increased burial time and temperature above about 75-90 ^oC (along with other factors) is also well established (Giles et. al., 2000).

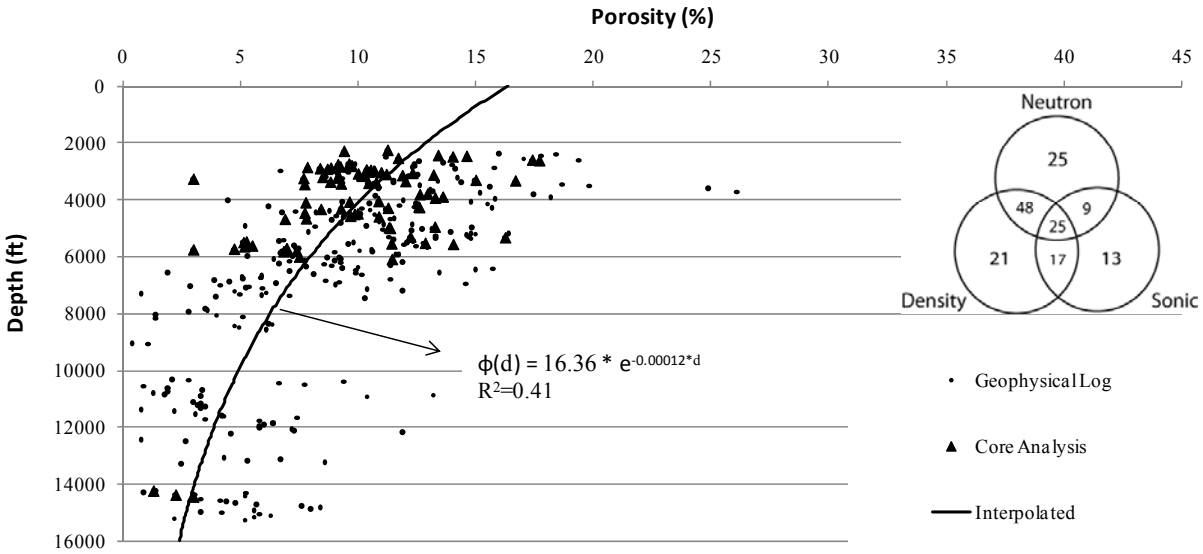

Figure 7. Exponential regression between depth and porosity data from core analyses (40 wells) and geophysical logs (158 wells) of the Mount Simon Sandstone. The Venn diagram illustrates the number of wells having geophysical logs for porosity.

4.2. NET POROSITY-FEET

A crucial parameter used to calculate the theoretical storage capacity within a given area is the usable pore volume, here denoted as net porosity feet. This parameter is defined as the portion of the gross reservoir that consists of the porosity value (expressed as a percentage, where porosity measured by geophysical logs is equal or greater than 7% and gamma ray values are lower than 75 API (equations 6 and Figure 9 illustrate this) multiplied by net thickness. Alternatively, equation [3] along with depth information can be used to calculate the theoretical values of net porosity feet within the limits defined for the Mount Simon Sandstone (Figure 2). The net porosity feet at any location, where the top and the bottom of the Mount Simon Sandstone are z_{top} and ($z_{top}+\Delta z$) respectively, is:

$$\emptyset_{feet}(net)_{theoretical} = \int_{z_{top}}^{z_{top}+\Delta z} 0.01 * \emptyset(z)dz = \int_{z_{top}}^{z_{top}+\Delta z} 0.1636 * e^{-0.00012*z}dz \quad [4]$$

The solution of [4] is:

$$\emptyset_{feet}(net)_{theoretical} = 1{,}363.3 * \left(e^{-0.00012*z_{top}} - e^{-0.00012*(z_{top}+\Delta z)}\right) \quad [5]$$

where Δz is the thickness of the unit. Equation [5] incorporates the values of porosity and thickness and facilitates the calculation of the storage capacity at any given location in the MRCSP region. The values of net porosity feet were calculated using equation [5] for 135 well locations in the states of Kentucky, Indiana, Michigan, and Ohio, and compared to the values of net porosity from the geophysical logs at the same locations. We calculated net porosity feet from the geophysical logs using the algorithm:

$$\emptyset_{feet}(net)_{log} = \begin{cases} \sum_i d_i * \emptyset_i \ , & GR \leq 75 \text{ and } \emptyset_i \geq 7 \text{ percent} \\ 0 \ , & GR \geq 75 \text{ or } \emptyset_i \leq 7 \text{ percent} \end{cases} \quad [6]$$

where d_i is the distance of the interval at which the porosity $\emptyset_i$ is measured. In order to exclude clay and shale, a maximum value of 75 API units on the gamma ray log was chosen as the cutoff for calculating net porosity feet values. This threshold may not be always accurate because sandstones with higher content of K-feldspar may also result in higher gamma ray values. Coupling this threshold with a porosity cutoff value of 7 percent will provide an underestimation of effective porosity and calculated storage capacity. We observed a high correlation (r^2=0.9155) when comparing theoretical (equation [5]) versus measured (equation [6]) values for net porosity feet (Figure 8). The high correlation value may be a result of the fact that the equation derived for porosity and depth combined both core data and geophysical logs, implying that these two estimates are partially interdependent. Nevertheless, comparing measured data with theoretical values provides a preliminary evaluation of the assertiveness of the relationship established for porosity and depth.

Two locations were chosen where the Mount Simon and its correlatives occur at different depths to illustrate the effects of depth on porosity and on the value of net porosity feet. The first well is located in Ottawa County, Michigan and exhibits almost 98 ft of net porosity within a gross interval thickness of 951 ft. The second is a deep well in Webster County, Kentucky (which may be a sandstone older than the Mt Simon in the Rough Creek Graben) that contains less than 3 ft of net porosity out of a gross interval thickness of 330 ft. Comparing the ratios between net porosity and thickness of the basal sandstone in both locations led to 10 percent and 0.7 percent for average porosity, respectively (Figure 9).

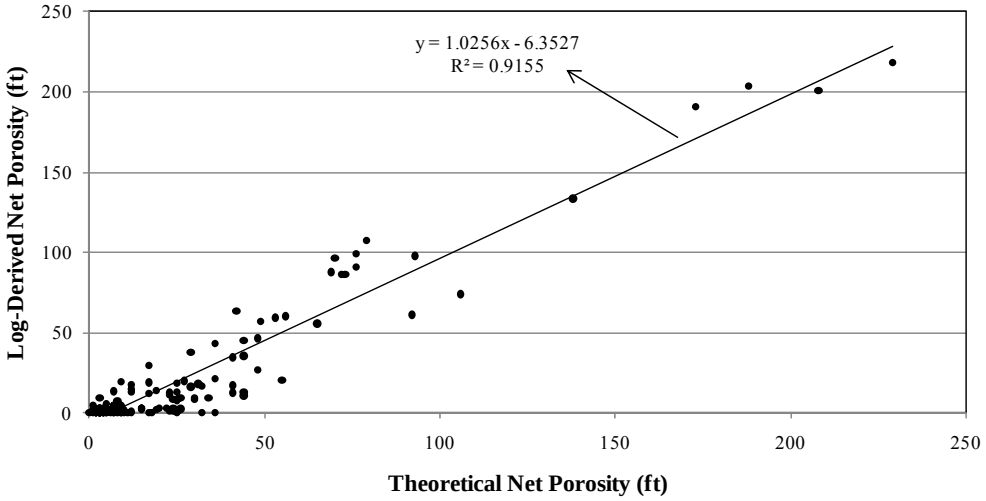

Figure 8. Net porosity values for the Mount Simon and other basal sandstones calculated from geophysical logs exhibit a high correlation with theoretical values derived from equation [3]. The plot contains data from 135 wells in the four states defined in this study.

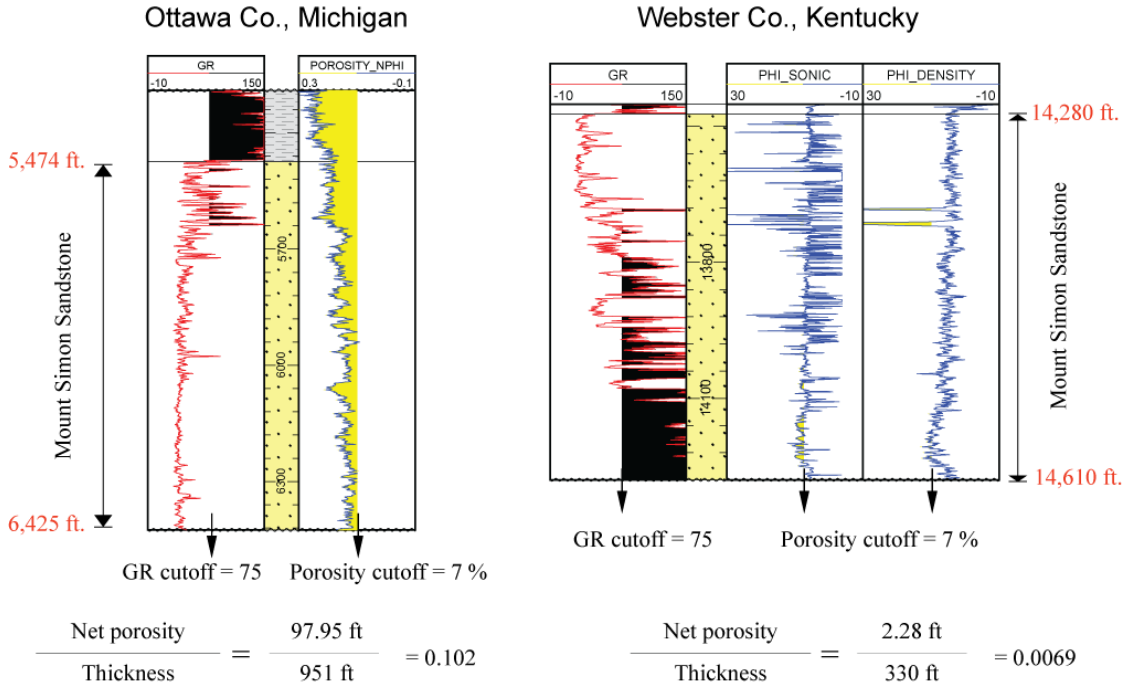

Figure 9. The relationship of net porosity with depth in two basal sandstone wells. Porosity is dramatically diminished with depth.

4.3. PERMEABILITY-POROSITY RELATIONSHIP

Core analyses from 2,472 samples taken from Kentucky (8 data points), Indiana (1,875 data points), Michigan (458 data points), and Ohio (131 data points) indicate a positive relationship between porosity and permeability (Figure 10). The correlation coefficient for this relationship was low (r^2=0.255). However, further examination of this relationship indicates that it could be better described by an exponential function defined by the equation:

$$k(\emptyset) = 0.7583 * e^{0.283 * \emptyset}; \; r^2 = 0.255 \qquad [7]$$

where k is permeability in millidarcies (md) and $\emptyset$ is porosity (percent). This equation may be useful for predicting the magnitude of permeability within the reservoir at a given depth when other data is lacking. This is an important start because the Mount Simon is being looked at as the major sequestration target in many parts of the region, but there are relatively few data points for the Mount Simon and its equivalents in many areas. The equation may also be useful for building preliminary flow models, where other data is lacking, although the low coefficient of correlation indicate that permeability varies widely (up to three orders of magnitude) for any given porosity. For instance, a value of 7 percent porosity predicts a permeability value of 5.5 md. However, core analyses show values that range from 0.1 to 100 md. CO_2 has relative permeability intermediate between liquid hydrocarbon and typical natural gas. Longstanding industry default (net-reservoir) cut-offs of 0.1 md for gas reservoirs, and 1.0 md for oil reservoirs are typically used in "net pay" calculations (Worthington and Cosentino, 2005). Assuming that 5 md corresponds to reservoir properties of 7 percent porosity (equation [7]), our approach to calculate net porosity from geophysical logs constitutes a conservative methodology.

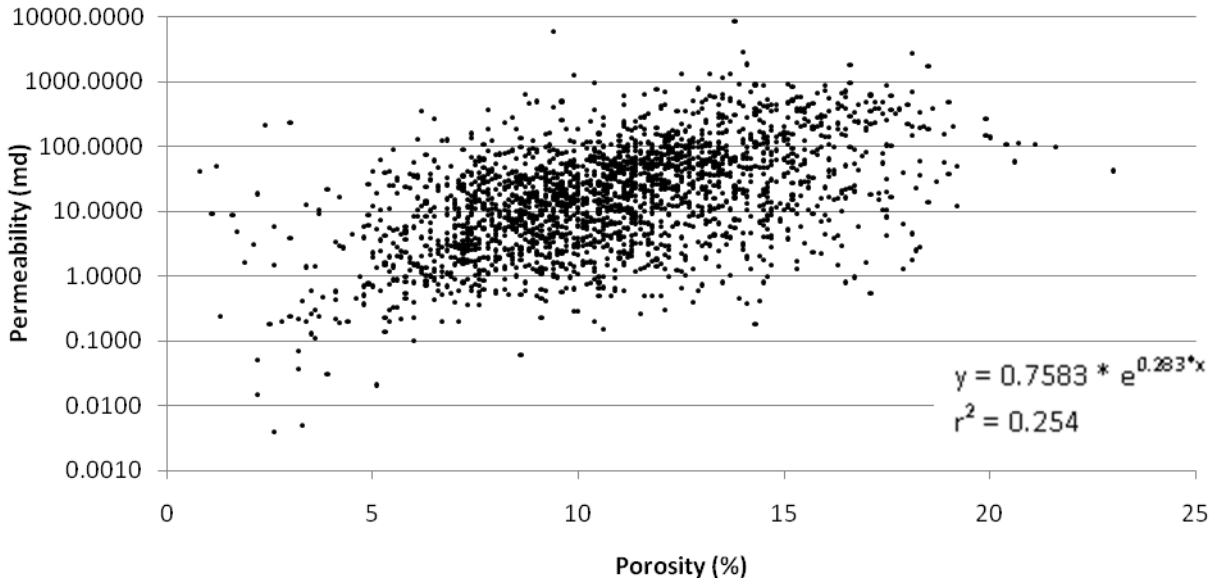

Figure 10. Semilog plot of permeability and porosity data collected at the MRCSP region.

Understanding the relationship of permeability and depth would also help in evaluating reservoir efficiency. Unfortunately, core data with information on permeability and depth shows a very low correlation (r^2=0.0171) between these two variables and do not allow us to establish a direct relationship.

4.4. REGIONAL DISTRIBUTION OF NET POROSITY AND STORAGE CAPACITY

A regional map with net porosity distribution in the Mount Simon Sandstone (Figure 11) was estimated using 135 gamma ray logs and porosity logs (neutron, sonic, and/or density). This map excludes correlative or older basal sandstones which fundamentally lie outside of the area with recognized Mount Simon sandstones. The net porosity map, along with the methodology for estimating CO_2 storage capacity in deep saline aquifers allows the calculation of a preliminary estimation of the CO_2 storage capacity in the pore space of this reservoir.

Maximum net porosity was determined for the Mount Simon in a well in northern Indiana (Bethlehem Steel WD#1, Porter Co. Indiana), while several wells in the central and northern Michigan basin, Ohio, and Kentucky have little or no effective porosity, despite substantial stratigraphic thickness, and are therefore unsuitable for CO_2 injection. Following the calculation of net porosity, we estimated the storage capacity for each county by using the following relationship:

$$SC = \emptyset_h * \rho_{CO2} * \xi * A * C \qquad [8]$$

where SC = CO_2 storage capacity in metric tons; $\emptyset_h$ = net porosity; ρ_{CO2} = CO_2 density (a constant value of 767 kg/m^3 [47.92 lbs/ft^3] was used for all depths); ξ = storage efficiency of 1%, 4%, 10% and 15%; A = area in km^2; and C = a constant for unit conversion to metric tons. The resultant values for storage capacity in each portion of the four-state region indicated in Figure 2 are listed in Table 2. For a detailed list of counties with their associated values of net porosity and storage capacity using efficiency factors of 1, 5, 10, and 15%, see Appendix 1.

Table 2: Summary of resultant storage capacity per state. The area considered in this assessment is in agreement with figures 2, 11, and 12.

State	Area (km^2)	Net Porosity (ft)	Storage Capacity (MM Tons CO_2)*	Storage Capacity per Unit of area (MM Tons/Km^2)*	Storage Capacity including efficiency factor (MM Tons CO_2)			
					ξ = 1%	ξ = 5%	ξ = 10%	ξ = 15%
Indiana	49,649	116.14	1,475,765	29.72	14,753	73,787	147,579	221,363
Michigan	38,793	69.58	632,498	16.30	6,326	31,627	63,248	94,874
Kentucky	19,141	17.83	73,683	3.85	738	3,687	7,369	11,054
Ohio	51,592	15.51	186,343	3.61	1,863	9,317	18,636	27,951
Total	159,175	54.76 (mean)	2,368,289	14.88	23,680	118,418	236,832	355,242

* These values are total and therefore do not include ξ.

For the solely purpose of comparing our estimates with those published (DOE/NETL, 2008), we estimated the storage capacity assuming that all the pore spaces of the Mount Simon Sandstone can store CO_2. We used efficiency factors of 1% and 4%, and estimated that the total amount of carbon dioxide that can be stored in the area defined for the Mount Simon Sandstone

is 37.8 and 151.2 billion metric tons of CO_2, respectively. This is approximately 74 percent higher than the values of 21.7 and 86.9 billion metric tons of CO_2 estimated by the MRCSP for the capacity of the Mount Simon Sandstone in the states of Indiana, Kentucky, Michigan, and Ohio.

A critical term in the calculation shown in equation [8] is storage efficiency, ξ. This parameter is obtained by multiplying a combination of volumetric and reservoir performance parameters that reflect what portion of the subsurface will actually be occupied by carbon dioxide and how that CO2 will move through the reservoir. The volumetric portion of ξ takes into account three factors: gross thickness to net thickness, total porosity to effective porosity, and total area to net area in the basin that has a suitable formation for injection. The following equation was used to estimate the storage efficiency factor for saline formations (DOE/NETL, 2008):

$$\xi_{saline} = \left(\frac{A_n}{A_t}\right) * \left(\frac{h_n}{h_g}\right) * \left(\frac{\phi_e}{\phi_{tot}}\right) * E_A * E_I * E_g * E_d \qquad [9]$$

where A_n/A_t is the fraction of total basin or regional area that has a suitable formation present; h_n/h_g is the fraction of total geologic unit that meets minimum porosity and permeability requirements for injection; $ø_e/ø_{tot}$ is the fraction of total porosity that is effective, i.e., interconnected; the last four factors in the equation (E_A, E_I, E_g, and E_d) represent how the reservoir will behave when injected with CO_2 and are values of areal displacement efficiency, vertical displacement efficiency, gravity or buoyancy efficiency, and microscopic displacement efficiency, respectively. The first three parameters are terms used to define the pore volume of the entire region, whereas the last four terms are used to describe the performance of the pore volume immediately adjacent to a single well injection. Appendix B in The Carbon Sequestration Atlas of the United States and Canada (DOE/NETL, 2008) present an extensive discussion of these storage efficiency factors and their use in making regional storage capacity calculations and suggest that a range of values between 1-4% for overall efficiency is appropriate for calculating capacity when values of total formation thickness, average porosity, and a complete regional area are used rather than net values of thickness, porosity and area. The approach used in this analysis incorporates a substantial decrease in uncertainty through consideration of net thickness, porosity, and area calculated from specific wells and regional patterns in the reservoir quality rock in the basal sandstone interval. Therefore, the calculations used in this analysis have assumed that the first three terms of equation [9] are equal to one. This approximation allows us to work with values of efficiency factors (ξ) of 10% and 15% in addition to 1% and 4% as presented by the atlas (See Appendix 1). With these modifications to the overall value of ξ, additional Monte Carlo simulations may be useful in order to better estimate more accurate values for ξ. A map of calculated CO_2 storage capacity, by county (Figure 12) indicates that the highest potential for geologic sequestration resides in the areas with higher net porosity in southwestern Michigan and northwestern Indiana.

Future work including the determination of storage capacity assessments at a site-scale and better understanding of internal facies and potential compartmentalization will facilitate an increase of the values of the storage efficiency factor used in the estimations for the Mount Simon geologic carbon sequestration capacity. And as the magnitude of the uncertainty is data density dependent, a lowering of uncertainty in the area immediately surrounding a well-

characterized borehole is justified but an overall decrease in the uncertainty is possible if systematic relationships of porosity and permeability are further established.

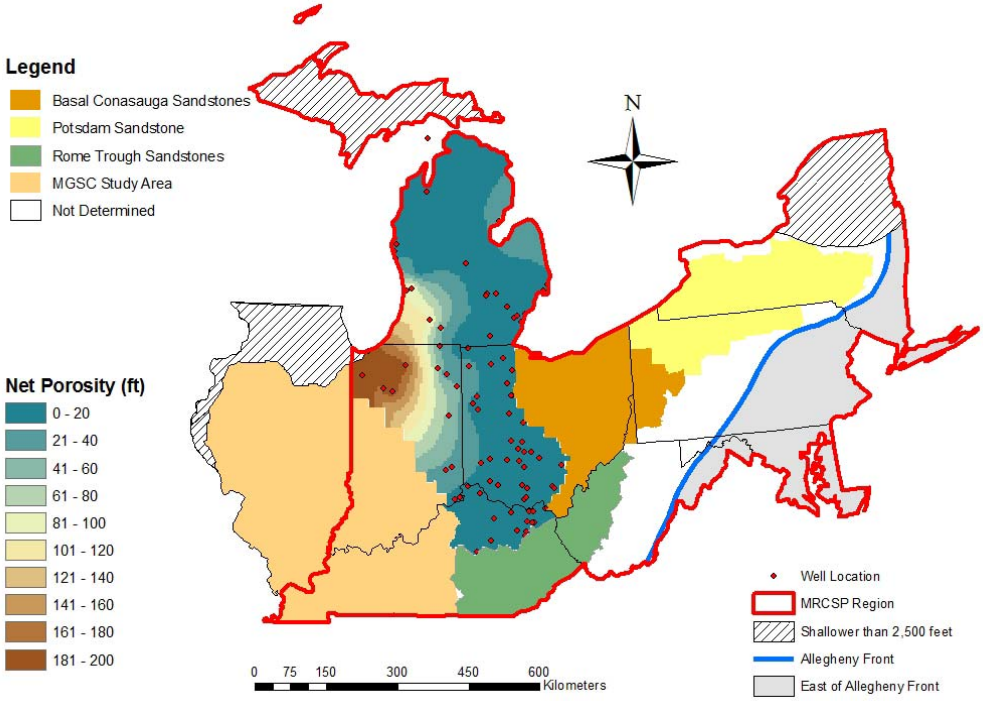

Figure 11. Net porosity feet distribution in the Mount Simon Sandstone. The raster was obtained from the interpolation from 128 points from wells with geophysical logs of gamma ray and porosity.

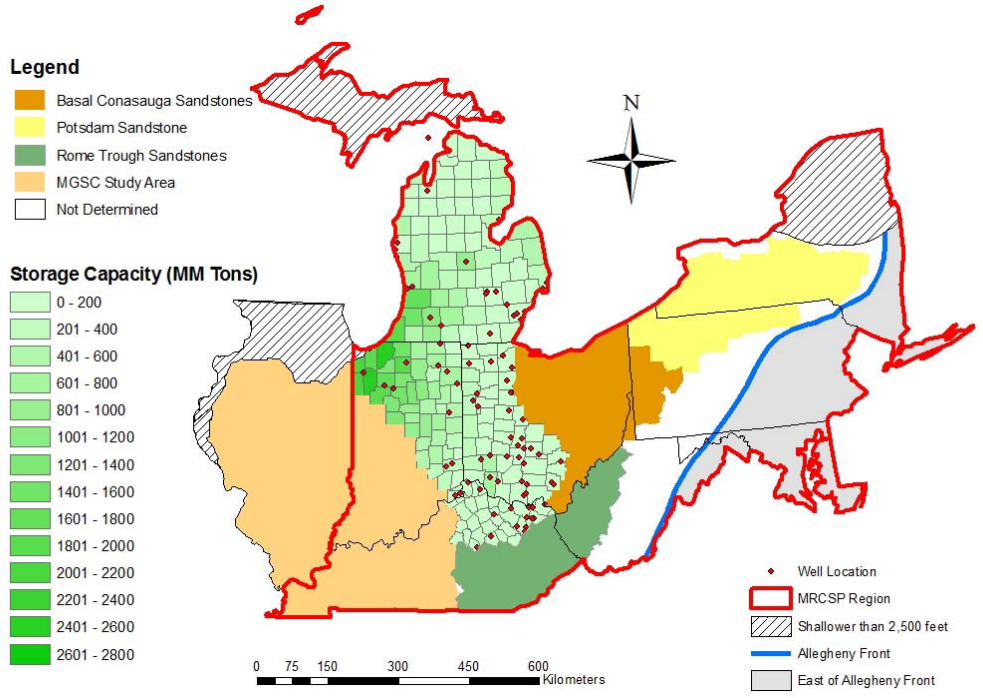

Figure 12. Storage capacity calculated by county using an efficiency factor of 4 percent (ξ =4%) in the Mount Simon Sandstone.

5. DISCUSSION

Interpretation of the core and log derived porosity data from four states of the MRCSP region (Indiana, Kentucky, Michigan, and Ohio) indicates that there is a relationship between porosity and depth as previously identified by Hoholick et al., (1984) for only the Illinois basin. Across this portion of the MRCSP region, porosity appears to diminish exponentially with depth suggesting that porosity generally decreases to values of less than 7 percent at depths greater than 7,000 ft. Areas below this depth may not be suitable for the effective sequestration of CO_2. This general trend is consistent with the work of Hoholick et al. (1984) and the data compiled by Bowersox (2008, personal communication). However, the data compiled by these authors are from Mount Simon Sandstone samples primarily from the Illinois basin. The samples evaluated in this work were from Indiana, Kentucky, Michigan, and Ohio, and complement the previous knowledge of porosity and depth relationships defined initially in Illinois. There is a need for additional samples and analyses from the deep portions of the Appalachian basin in New York, Pennsylvania, and West Virginia in order to extend the correlations defined in this study into the other basal sandstones in the eastern portion of the MRCSP region. Additionally, the regional distribution of the data and the differing lithologies found in the Mount Simon Sandstone and other basal sandstones throughout the entire study area may be responsible for the apparent high variability in porosity in the different wells.

There is no single relationship between porosity and permeability that is applicable to all porous media (Bloch, 1991; Pittman, 1992; Bloch et al., 2002). Not all of the pore spaces are equally effective in conducting fluid flow. Two rocks with the same porosity, but with a different pore structure, can have different pore space efficiency and therefore different permeabilities (Bernabé et al., 2003). From a carbon sequestration standpoint, porosity is a key factor in determining the volumetric potential for CO_2 storage, whereas permeability is an indicator of the reservoir efficiency for CO_2 flow in the porous media.

The low correlation coefficient (r^2=0.41) obtained for porosity and depth, and the very low correlation coefficients obtained for permeability-porosity and permeability-depth relationships (r^2 = 0.254 and r^2 = 0.0171, respectively) may be indicative of heterogeneities that are present in the subsurface environment that have resulted from geological complexities beyond simple porosity and permeability reduction by quartz overgrowth and pressure solution/deposition. The data used in this study were from multiple wells located at considerable distance (different populations), which likely contributed to the low regression coefficient. Higher coefficients might be derived by examining subsets of the data that were more geographically restricted. Any effort to establish a unique relationship between petrophysical properties and depth must be conducted separately for each group of wells based on geological criteria. Heterogeneities within the Mount Simon caused by variations in the primary depositional environment and diagenetic history also likely contribute to the low regression coefficient. The combination of different depositional environments and diagenetic histories (in different basins) has resulted in complex patterns in internal stratigraphy, mineralogy and diagenetic fabric. Some of the data included in the analyses may also be from Cambrian sandstones that are actually older than the Mount Simon and would have potentially different depositional histories. Therefore, a detailed characterization of this and other basal sandstones is necessary before establishing a more comprehensive predictive relationship for porosity or

permeability. The distribution of stratigraphic units within the basal sandstone across the region and their associated petrophysical attributes need to be established for effective prediction of these parameters. Additionally, a careful vertical and lateral documentation of the composition of the reservoir needs to be conducted to define variation in mineralogy and stratigraphy.

The performance of this sandstone as a reservoir including the vertical displacement of injected fluids from buoyancy forces and the horizontal displacement of CO_2 will be directly controlled by the distribution of porosity and permeability. To realistically simulate reservoir performance, predictive flow modeling will need to take into account these heterogeneities in the sandstone when incorporating petrophysical parameters of porosity and permeability into the simulation.

The main filters applied to calculate net porosity at each individual well (a 7% porosity cutoff and a maximum GR log response of 75) eliminate inferred, non-sandstone lithology. K-feldspar and glauconite may, in part, explain higher GR log responses in wells in this area. The results of regional net porosity calculations are, therefore, considered conservative estimates of regional storage capacity. Our resultant estimates of storage capacity are approximately 20% lower than the values published by the Carbon Sequestration Atlas of the United States and Canada (DOE/NETL, 2008, p. 54).

Several important relationships are supported by the net porosity map shown in Figure 11. Net porosity (or porosity/feet, $Ø_h$ in units of ft^3/ft^2) is, in part, consistent with formation isopach thickness but is profoundly modified by porosity reduction due to deep burial-induced (>6,500ft; 1981m). Moderate, to poor reservoir quality and significant thinning of the Mount Simon where buried to a moderate depth results in modest net porosity values in southeastern Michigan, Ohio, and northern Kentucky (Figure 11, 12, and Appendix I).

6. CONCLUSIONS

The Upper Cambrian Mount Simon Sandstone and other basal sandstones in the MRCSP region may function as an effective sink for injected carbon dioxide because of its lateral continuity, its thickness, and its high porosity. A dramatic decrease in porosity at burial depths below 7,000 ft implies that there is little or no storage capacity in the Mt. Simon Sandstone in portions of the region where the unit lies at depths of more than 7,000 ft. Estimates, using wireline log data from regional wells, indicate that the potential for geological carbon storage capacity is greatest in the southwestern Michigan and northwestern Indiana. This area corresponds to thick, favorable sedimentary facies and relatively shallow burial depths where only modest diagenetic modification of reservoir quality has occurred.

Regression analyses using core and log data, primarily from the western portion of the region, indicate that there is an inverse relationship between porosity and depth. At depths above 7,000 ft the Mount Simon Sandstone appears to have sufficient porosity for industrial-scale storage. These results confirm earlier depth-porosity relationships in the Illinois basin and expand them into other parts of the MRCSP region. From these analyses, net porosity maps were generated for the Mount Simon in the MRCSP region. There is also a positive porosity-

permeability relationship for the Mount Simon Sandstone, although it has a low correlation coefficient.

Although the equations and results derived in this study should prove useful for regional analyses of this important potential reservoir, it must be remembered that these represent regional averages with significant local variability. A relative lack of data from depths below 7,000 ft and from the eastern portion of the region indicates that there still remains a high degree of uncertainty in the depth-porosity correlation in this portion of the region. Additionally, mineralogical and textural heterogeneities that occur within the reservoir that are controlled by variations in the source material, depositional environments, and subsequent diagenetic processes complicate the depth-decreasing porosity relationship which is fundamentally a quartz-overgrowth constrained phenomenon. Log-derived porosity could be used to estimate permeability and reduce this uncertainty in the deepest part of the basins, and in correlative and older sandstones, but there is a low correlation coefficient between permeability and porosity, so more work will be needed to determine the relationship between permeability, porosity, and depth. These should include investigating all types of pore-filling material including an analysis of other types of cementation. Future studies should incorporate three dimensional facies characterization and investigate the role that lithologic variability plays in reservoir quality. To this end, petrological analysis of core and sidewall cores from the Phase II East Bend demonstration project is beginning at this time. These data will help to confirm some of the general regional trends that have been presented in this report and also help to reduce the uncertainty and further define the petrophysical character of the flow units within the Mount Simon at this locality on the Cincinnati Arch.

Additional work is needed to define internal units within the basal sandstone and use these subdivisions to better characterize and therefore effectively predict the lateral and vertical extent of porosity. There may be units that are correlative across large areas, or there may be significant internal heterogeneity, that would influence the ability to apply regional predictions. The relationship of non-quartz phases in the section and their control on the presence or absence of porosity and associated permeability needs also to be refined. If some of these analyses can be undertaken and results refined, the degree of confidence that can be assigned to estimating reservoir properties and performance from the available regional data will be greatly enhanced.

7. REFERENCES

Ammerman, M. L. and G. R. Keller, 1979, Delineation of Rome Trough in eastern Kentucky by gravity and deep drilling data. AAPG Bulletin, 63, p. 341-353.

Asquith, G. and D. Krygowski, 2004, Porosity Logs: *in* G. Asquith and D. Krygowski, Basic Well Log Analysis: AAPG Methods in Exploration 16, p. 37–76.

Baranoski, M.T., 2007, Is the Cambrian Mount Simon a regional "blanket sandstone" across Ohio? 2007 AAPG Annual Convention and Exhibition (April 1 - 4, 2007) Technical Program, http://aapg.confex.com/aapg/2007am/techprogram/A110203.htm.

Barnes, D. A., D. H. Bacon, and S. R. Kelley, 2009, Geological sequestration of carbon dioxide in the Cambrian Mount Simon Sandstone: Regional storage capacity, site characterization, and large-scale injection feasibility, Michigan Basin: Environmental Geosciences, v. 16, p. 163-183.

Bernabé, Y., U. Mok, and B. Evans, 2003, Permeability-porosity relationships in rocks subjected to various evolution processes: Pure Applied Geophysics, v. 160, p. 937-960.

Bloch, S., 1991, Empirical prediction of porosity and permeability in sandstones: AAPG Bulletin, v. 75, p. 1145-1160.

Bloch, S., R. H. Lander, and L. Bonnell, 2002, Anomalously high porosity and permeability in deeply buried sandstone reservoirs: origin and predictability: AAPG Bulletin, v. 86, p. 301-328.

DOE/NETL, 2008, Carbon Sequestration Atlas of the United States and Canada (Atlas II), Online ed. National Energy Technology Laboratory, Morgantown, WV, http://www.netl.doe.gov/technologies/carbon_seq/refshelf/atlasII/atlasII.pdf.

Driese, S. G., C. W. Byers, and R. H. Dott, 1981, Tidal deposition in the basal Upper Cambrian Mt. Simon Formation in Wisconsin: Journal of Sedimentary Research, v. 51, p. 367-381.

Hoholick, J. D., T. Metarko, and P. E. Potter, 1984, Regional variations of porosity and cement: St. Peter and Mount Simon Sandstones in Illinois basin: AAPG Bulletin, v. 68, p. 753-764.

Giles, M. R., S. L. Indrelid, G. V. Beynon, and J. Amthor, 2000, The Origin of Large-Scale Quartz Cementation; Evidence From Large Data Sets and Coupled Heat-Fluid Mass Transport Modeling: *in* Richard H. Worden and Sadoon Morad, eds., *Quartz Cementation in Sandstones,* Special Publication of the International Association of Sedimentologists, no. 29, pp. 21-38.

Harris, D.C., Drahovzal, J.A., Hickman, J.G., Nuttall, B.C., Baranoski, M.T., and Avary, K.L., 2004, Rome Trough Consortium final report and data distribution: Report submitted to industry partners and to the U.S. Department of Energy in fulfillment of U.S. Department

of Energy contract DE-AF26-98FT02147, Kentucky Geological Survey, ser. XI, Open-file Report 5875, varied pagination, 1 CD-ROM.

Hickman, J.B., and Harris, D.C., 2004, Chapter 6-Homer Field Study: *in* Harris, D.C., Drahovzal, J.A., Hickman, J.G., Nuttall, B.C., Baranoski, M.T., and Avary, K.L., eds., Rome Trough Consortium final report and data distribution: Report submitted to industry partners: Kentucky Geological Survey, ser. XI, Open-file Report 5875, 16 p.

Howell, P. D., and B. A. van der Pluijm, 1999, Structural sequences and styles of subsidence in the Michigan basin: Geol. Soc. Am. Bull., v. 111, p. 974-991.

IPCC—Intergovernmental Panel on Climate Change, 2005: *in* Metz, B., Davidson, O., de Coninck, H.C., Loos, M., Meyer, L.A. (Eds.), Special Report on Carbon Dioxide Capture and Storage. Cambridge University Press, Cambridge, UK and New York, NY, USA, Chapter 5, pp. 195–276.

Lemmon, E. W, M. O. McLinden, and D. G. Friend, 2008, Thermophysical Properties of Fluid Systems, in NIST Chemistry WebBook, NIST Standard Reference Database Number 69, Eds. P.J. Linstrom and W.G. Mallard, National Institute of Standards and Technology, Gaithersburg MD, 20899, <http://webbook.nist.gov> Accessed May 26, 2009.

Makowitz, A., R. H. Lander, and K. L. Milliken, 2006, Diagenetic modeling to assess the relative timing of quartz cementation and brittle grain processes during compaction: AAPG Bulletin, v. 90, p. 873-885.

Makowitz, A. and K. L. Milliken, 2003, Quantification of brittle deformation in burial compaction, Frio and Mount Simon Formation sandstones: Journal of Sedimentary Research, v. 73, p. 1007-1021.

Martin, F. D., R. P. Kendall, E. M. Whitney, B. A. Hardage, B. A. Stubbs, B. Uszynski, and W.W. Weiss, 1999, Advanced reservoir characterization for improved oil recovery in a New Mexico Delaware basin project, in R. A. Schatzinger and J. F. Jordan, eds., Reservoir Characterization-Recent Advances: AAPG Memoir 71, p. 93-108.

Medina, C., Barnes, D., and Rupp, J., 2008, Depth relationships in porosity and permeability in the Mount Simon Sandstone of the Midwest region: applications for carbon sequestration: Eastern Section Meeting of the American Association of Petroleum Geologists (Oct. 14).

Pittman, E. D., 1992, Relationship of porosity and permeability to various parameters derived from mercury injection-capillary pressure curves for sandstone: AAPG Bulletin, v. 76, p. 191-198.

Ryder, R. T., 1991, Stratigraphic framework of Cambrian and Ordovician rocks in the Central Appalachian basin from Richland County, Ohio, to Rockingham County, Virginia; revised and digitized by Robert D. Crangle, Jr.: U.S. Geological Survey Miscellaneous Investigations Series Map I-2264, online version 1.0. http://pubs.usgs.gov/imap/i-2264/

Schlumberger, 1972, Log interpretation, volume I – principles: New York, Schlumberger Publication, 113 p.

Selley, R. C., 1978, Porosity gradients in North Sea oil-bearing sandstones: Journal of the Geological Society of London, v. 135, p. 119-132.

Shrake, D. L., 1991, The Middle Run Formation: a subsurface stratigraphic unit in Southern Ohio. Ohio Journal of Science, v. 91, p. 49-55.

Shrake, D. L., R. W. Carlton, and L. H. Wickstrom, 1991, Pre-Mount Simon basin under the Cincinnati Arch: Geology, 19, p. 139-142.

Sloss, L. L, 1963, Sequences in the Cratonic Interior of North America Geological Society of America Bulletin v. 74: pp. 93-114.

Solomon, S., 2006, Carbon dioxide storage: geological security and environmental issues - case study on the Sleipner gas field in Norway, The Bellona Foundation, Oslo, Norway: http://bellona.no/filearchive/fil_Paper_Solomon_-_CO2_Storage.pdf [accessed January 12, 2009].

Walcott, C. D., 1914, Cambrian geology and paleontology: Smithsonian Misc. Coll., v. 57, p. 345-412.

Wickstrom, L. H., M. T. Baranoski, D. M. Powers, J. B. Hickman, W. Solano, C. P. Korose, 2003, Generalized contour maps of the Sauk Sequence in Illinois, Indiana, Kentucky and Ohio. Basic tools for the characterization of saline aquifers for CO_2 sequestration: *in* Kansas Geological Survey Open File Rpt, 2003-33, online version, http://www.kgs.ku.edu/PRS/publication/2003/ofr2003-33/P3-07.html

Wickstrom, L. H., E. R. Venteris, J. A. Harper, J. McDonald, E. R. Slucher, K. M. Carter, S. F. Greb, J. G. Wells, W. B. Harrison III, B. C. Nuttall, R. A. Riley, J. A. Drahovzal, J. A. Rupp, K. L. Avary, S. Laham, D. A. Barnes, N. Gupta, M. A. Baranoski, P. Radhakrishnan, M. P. Solis, G. R. Baum, D. Powers, M. E. Hohn, M. P. Parris, K. McCoy, G. M. Grammer, S. Pool, C. M. Luckhardt, and P. Kish, 2005, Characterization of geologic sequestration opportunities in the MRCSP region: Phase I task report period of performance: October 2003-September 2005, 152 p.

Willman, H. B., E. Atherton, T. C. Buschbach, C. Collinson, J. C. Frye, M. E. Hopkins, J. A. Lineback, and J. A. Simon, 1975, Handbook of Illinois stratigraphy: Illinois State Geological Survey Bulletin 95, 261 p.

Worthington, P. F. and L. Cosentino, 2005, The role of cutoffs in integrated reservoir studies: SPE Paper 84387-PA, SPE Reservoir Evaluation & Engineering, v. 8, p. 276-290.

8. APPENDICES

APPENDIX I. Net porosity and storage capacity calculated at each county in the Mount Simon Sandstone defined in Figure 2.

ID	County	State	Area (km^2)	Net Porosity (ft)	Storage Capacity (MM Tons CO_2)	ξ = 1%	ξ = 5%	ξ = 10%	ξ = 15%
1	Lake	Indiana	1275	297.04	89836	898	4492	8984	13475
2	Porter	Indiana	1127	256.76	68638	686	3432	6864	10296
3	Noble	Indiana	1097	118.26	30772	308	1539	3077	4616
4	De Kalb	Indiana	950	56.06	12633	126	632	1263	1895
5	Marshall	Indiana	1183	233.60	65551	656	3278	6555	9833
6	Kosciusko	Indiana	1462	188.62	65411	654	3271	6541	9812
7	Starke	Indiana	804	224.05	42728	427	2136	4273	6409
8	Whitley	Indiana	880	124.76	26042	260	1302	2604	3906
9	Jasper	Indiana	1430	249.71	84703	847	4235	8470	12705
10	Allen	Indiana	1773	65.74	27650	277	1382	2765	4148
11	Newton	Indiana	1069	275.20	69781	698	3489	6978	10467
12	Fulton	Indiana	945	207.91	46606	466	2330	4661	6991
13	Pulaski	Indiana	1095	222.26	57728	577	2886	5773	8659
14	Wabash	Indiana	1070	136.51	34646	346	1732	3465	5197
15	Huntington	Indiana	949	98.68	22213	222	1111	2221	3332
16	Miami	Indiana	945	158.58	35547	355	1777	3555	5332
17	Adams	Indiana	920	39.49	8619	86	431	862	1293
18	Wells	Indiana	940	63.40	14137	141	707	1414	2121
19	Cass	Indiana	1064	181.84	45894	459	2295	4589	6884
20	White	Indiana	1273	216.98	65519	655	3276	6552	9828
21	Carroll	Indiana	996	180.54	42654	427	2133	4265	6398
22	Grant	Indiana	1073	92.78	23613	236	1181	2361	3542
23	Blackford	Indiana	462	56.43	6184	62	309	618	928
24	Jay	Indiana	1041	30.13	7439	74	372	744	1116
25	Howard	Indiana	806	136.18	26035	260	1302	2604	3905
26	Clinton	Indiana	1057	150.87	37826	378	1891	3783	5674
27	Tipton	Indiana	646	115.68	17726	177	886	1773	2659
28	Madison	Indiana	1210	75.93	21793	218	1090	2179	3269
29	Delaware	Indiana	1061	49.62	12488	125	624	1249	1873
30	Randolph	Indiana	1199	20.83	5925	59	296	593	889
31	Hamilton	Indiana	1066	99.92	25266	253	1263	2527	3790
32	Henry	Indiana	1047	35.65	8853	89	443	885	1328
33	Wayne	Indiana	1087	16.11	4153	42	208	415	623
34	Hancock	Indiana	816	65.48	12674	127	634	1267	1901
35	Rush	Indiana	1117	37.15	9842	98	492	984	1476

APPENDIX I (Cont.)

ID	County	State	Area (km^2)	Net Porosity (ft)	Storage Capacity (MM Tons CO_2)	ξ = 1%	ξ = 5%	ξ = 10%	ξ = 15%
36	Fayette	Indiana	598	17.68	2508	25	125	251	376
37	Union	Indiana	484	13.32	1529	15	76	153	229
38	Shelby	Indiana	1102	65.93	17235	172	862	1724	2585
39	Franklin	Indiana	985	16.73	3909	39	195	391	586
40	Decatur	Indiana	937	46.05	10236	102	512	1024	1535
41	Dearborn	Indiana	857	29.06	5907	59	295	591	886
42	Ripley	Indiana	1143	39.48	10703	107	535	1070	1605
43	Ohio	Indiana	210	42.56	2120	21	106	212	318
44	Switzerlan	Indiana	601	47.88	6826	68	341	683	1024
45	La Porte	Indiana	1603	234.10	89014	890	4451	8901	13352
46	St. Joseph	Indiana	1157	228.71	62769	628	3138	6277	9415
47	Elkhart	Indiana	1204	191.66	54736	547	2737	5474	8210
48	Lagrange	Indiana	978	101.92	23643	236	1182	2364	3546
49	Steuben	Indiana	855	37.01	7505	75	375	751	1126
Total (Indiana)			49649	116.14	1475765	14753	73787	147579	221363
50	Mason	Michigan	1331	15.18	4793	48	240	479	719
51	Oceana	Michigan	1402	25.66	8533	85	427	853	1280
52	Muskegon	Michigan	1331	40.64	12832	128	642	1283	1925
53	Ottawa	Michigan	1532	86.63	31481	315	1574	3148	4722
54	St. Clair	Michigan	1851	32.32	14190	142	710	1419	2129
55	Macomb	Michigan	1246	15.97	4719	47	236	472	708
56	Oakland	Michigan	2373	33.05	18606	186	930	1861	2791
57	Livingston	Michigan	1486	17.45	6152	62	308	615	923
58	Allegan	Michigan	2241	134.80	71659	717	3583	7166	10749
59	Eaton	Michigan	1494	48.52	17194	172	860	1719	2579
60	Barry	Michigan	1474	84.49	29541	295	1477	2954	4431
61	Wayne	Michigan	1594	26.08	9862	99	493	986	1479
62	Washtenav	Michigan	1891	39.51	17721	177	886	1772	2658
63	Jackson	Michigan	1898	25.02	11263	113	563	1126	1689
64	Kalamazoo	Michigan	1501	138.70	49382	494	2469	4938	7407
65	Calhoun	Michigan	1857	62.54	27549	275	1377	2755	4132
66	Van Buren	Michigan	1636	174.95	67891	679	3395	6789	10184
67	Berrien	Michigan	1541	218.79	79976	800	3999	7998	11996
68	Monroe	Michigan	1512	33.63	12063	121	603	1206	1809
69	Lenawee	Michigan	1991	25.87	12218	122	611	1222	1833

APPENDIX I (Cont.)

ID	County	State	Area (km^2)	Net Porosity (ft)	Storage Capacity (MM Tons CO_2)	ξ = 1%	ξ = 5%	ξ = 10%	ξ = 15%
70	Hillsdale	Michigan	1588	19.42	7317	73	366	732	1098
71	Branch	Michigan	1351	50.55	16200	162	810	1620	2430
72	St. Joseph	Michigan	1341	130.76	41593	416	2080	4159	6239
73	Cass	Michigan	1331	189.29	59763	598	2988	5976	8964
Total (Michigan)			38793	69.58	632498	6326	31627	63248	94874
74	Boone	Kentucky	644	34.40	5255	53	263	526	788
75	Campbell	Kentucky	398	31.68	2991	30	150	299	449
76	Kenton	Kentucky	426	34.16	3451	35	173	345	518
77	Pendleton	Kentucky	737	30.70	5367	54	268	537	805
78	Gallatin	Kentucky	256	45.73	2777	28	139	278	417
79	Bracken	Kentucky	529	19.23	2413	24	121	241	362
80	Grant	Kentucky	676	38.00	6093	61	305	609	914
81	Carroll	Kentucky	342	46.56	3777	38	189	378	567
82	Mason	Kentucky	605	8.08	1160	12	58	116	174
83	Greenup	Kentucky	887	6.26	1317	13	66	132	198
84	Owen	Kentucky	932	37.04	8188	82	409	819	1228
85	Lewis	Kentucky	1216	2.77	800	8	40	80	120
86	Robertson	Kentucky	275	17.13	1118	11	56	112	168
87	Harrison	Kentucky	796	23.43	4424	44	221	442	664
88	Fleming	Kentucky	929	4.65	1026	10	51	103	154
89	Carter	Kentucky	1063	11.26	2840	28	142	284	426
90	Boyd	Kentucky	416	3.35	331	3	17	33	50
91	Scott	Kentucky	747	22.92	4060	41	203	406	609
92	Nicholas	Kentucky	519	11.66	1436	14	72	144	215
93	Rowan	Kentucky	761	2.77	500	5	25	50	75
94	Franklin	Kentucky	537	23.02	2932	29	147	293	440
95	Bourbon	Kentucky	738	11.13	1948	19	97	195	292
96	Bath	Kentucky	735	4.08	712	7	36	71	107
97	Fayette	Kentucky	761	13.37	2413	24	121	241	362
98	Montgome	Kentucky	520	2.71	335	3	17	34	50
99	Woodford	Kentucky	497	14.11	1663	17	83	166	249
100	Anderson	Kentucky	547	12.81	1662	17	83	166	249
101	Clark	Kentucky	661	4.94	774	8	39	77	116
102	Menifee	Kentucky	548	5.84	759	8	38	76	114
103	Jessamine	Kentucky	443	11.05	1161	12	58	116	174
Total (Kentucky)			19141	17.83	73683	738	3687	7369	11054

APPENDIX I (Cont.)

ID	County	State	Area (km^2)	Net Porosity (ft)	Storage Capacity (MM Tons CO_2)	ξ = 1%	ξ = 5%	ξ = 10%	ξ = 15%
104	Lucas	Ohio	873	13.03	2699	27	135	270	405
105	Fulton	Ohio	1054	10.39	2597	26	130	260	390
106	Williams	Ohio	1088	20.88	5389	54	269	539	808
107	Wood	Ohio	1596	5.57	2109	21	105	211	316
108	Henry	Ohio	1121	12.63	3359	34	168	336	504
109	Defiance	Ohio	1065	31.18	7876	79	394	788	1181
110	Paulding	Ohio	1084	36.89	9485	95	474	949	1423
111	Hancock	Ohio	1384	7.41	2433	24	122	243	365
112	Putnam	Ohio	1243	21.64	6382	64	319	638	957
113	Van Wert	Ohio	1052	30.67	7652	77	383	765	1148
114	Allen	Ohio	1033	17.32	4245	42	212	425	637
115	Hardin	Ohio	1211	8.84	2540	25	127	254	381
116	Mercer	Ohio	1238	15.30	4492	45	225	449	674
117	Auglaize	Ohio	1031	8.16	1996	20	100	200	299
118	Logan	Ohio	1222	6.34	1837	18	92	184	276
119	Union	Ohio	1100	8.94	2332	23	117	233	350
120	Shelby	Ohio	1048	4.97	1235	12	62	124	185
121	Darke	Ohio	1551	11.10	4084	41	204	408	613
122	Champaign	Ohio	1114	11.40	3011	30	151	301	452
123	Miami	Ohio	1039	12.31	3034	30	152	303	455
124	Franklin	Ohio	1442	8.47	2896	29	145	290	434
125	Madison	Ohio	1219	13.77	3981	40	199	398	597
126	Clark	Ohio	1029	17.42	4253	43	213	425	638
127	Fairfield	Ohio	1332	8.20	2591	26	130	259	389
128	Montgome	Ohio	1209	22.61	6483	65	324	648	972
129	Preble	Ohio	1107	19.89	5223	52	261	522	783
130	Greene	Ohio	1046	19.14	4748	47	237	475	712
131	Pickaway	Ohio	1307	8.58	2660	27	133	266	399
132	Fayette	Ohio	1049	18.81	4680	47	234	468	702
133	Hocking	Ohio	1105	6.28	1645	16	82	165	247
134	Warren	Ohio	1073	30.58	7784	78	389	778	1168
135	Butler	Ohio	1213	28.97	8336	83	417	834	1250
136	Clinton	Ohio	1100	21.87	5707	57	285	571	856
137	Ross	Ohio	1802	24.52	10480	105	524	1048	1572
138	Vinton	Ohio	1071	5.07	1289	13	64	129	193
139	Highland	Ohio	1421	18.39	6200	62	310	620	930

APPENDIX I (Cont.)

ID	County	State	Area (km^2)	Net Porosity (ft)	Storage Capacity (MM Tons CO_2)	ξ = 1%	ξ = 5%	ξ = 10%	ξ = 15%
140	Hamilton	Ohio	1083	27.90	7166	72	358	717	1075
141	Clermont	Ohio	1204	23.01	6571	66	329	657	986
142	Brown	Ohio	1271	8.18	2466	25	123	247	370
143	Jackson	Ohio	1091	5.81	1503	15	75	150	225
144	Pike	Ohio	1128	18.10	4844	48	242	484	727
145	Adams	Ohio	1536	8.92	3249	32	162	325	487
146	Scioto	Ohio	1607	7.35	2801	28	140	280	420
Total (Ohio)			51592	15.51	186343	1863	9317	18636	27951

APPENDIX II. Estimated deep saline formation for CO_2 storage capacity (published values). Table modified from DOE/NETL, 2008, p. 54).

Deep Saline Formation	Potential CO_2 Storage Resource (million metric tons CO_2)	
	Low Estimate (ξ=0.01)	High Estimate (ξ=0.04)
Mt. Simon Formation	21,700	86,900
St. Peter Sandstone	8,800	35,300
Medina/Tuscarora Sandstone	7,900	31,500
Rose Run Sandstone	5,700	23,100
Oriskany Sandstone	1,900	7,800
Sylvania Sandstone	1,500	6,000
Wastegate Formation	400	1,800
Basal Conasauga Sandstones	400	1,700
Potsdam Sandstone	1,200	4,500
Rome Trough Sandstones	100	500
TOTAL Deep Saline	**49,600**	**199,100**

Addendum – Cambrian

Eastern Cambrian Formation Results/Updates

The Mount Simon Sandstone was the main focus of the Cambrian formations because it represents such a large regional area with favorable reservoir properties and, therefore, a large portion of the potential saline reservoir CO_2 sequestration capacity. However, basal sands in the eastern portion of the study area such as the Potsdam and Rose Run Sandstones also have potential storage capacity, as determined and described during Phase I of MRCSP (Figure 1). This section describes the methods used to determine the storage capacity for these two formations because they are different than the methods used for the Mount Simon Sandstone. These methods are also consistent with the way the calculations used for the characterization of geologic sequestration opportunities in the Middle Devonian-Middle Silurian formations in the MRCSP region was carried out.

The general equation for volumetric storage CO_2-sequestration capacity involves determining the total pore volume, the percentage of the total pore volume space that CO_2 will occupy, and the density of CO_2 at reservoir temperature and pressure:

$$Q_{CO2} = E * \rho_{CO2} * \theta * A * H / 2200 \qquad (1)$$

where:

Q_{CO2} = CO_2 sequestration capacity (metric tonnes)
E = CO2-storage efficiency factor
ρ_{CO2} = Density of CO_2 under reservoir conditions (lbs/ft^3)
θ = Porosity (%)
A = Area (ft^2)
H = Thickness of the geologic sequestration unit (ft)
2200 = Conversion from lbs to metric tonnes

The percentage of the total pore volume that will be occupied by CO_2 is known as the efficiency factor. The efficiency factor accounts for several different geologic features that are physical barriers inhibiting the displacement of the native pore fluids by injected CO_2. These features can be grouped into terms that apply to an entire basin and terms that apply to a single injection well. Terms that apply to an entire basin include 1) the fraction of the total basin/region in which suitable formation present, 2) the fraction a of total geologic unit that has the minimum porosity and permeability, 3) and the fraction of total porosity that is interconnected. The factors that can be grouped into terms that apply to a single well include 1) the fraction of the immediate area surrounding an injection well that can be contacted by CO_2, 2) the fraction of the vertical cross section that can be contacted by CO_2, 3) the fraction of net thickness that is contacted by CO_2 as a consequence of the density difference between CO_2 and the pore fluids, 4) and the portion of the pore fluid volume that can be replaced by CO_2, which is directly related to the irreducible water saturation. The best estimate of the

efficiency factor is published by Capacity and Fairways Subgroup of the Geologic Working Group, U.S. DOE Regional Carbon Sequestration Partnerships (2007). The methodology for calculating capacity for the Cambrian formations is almost exactly the same methodology used for the MRCSP Phase I project, except that the efficiency factor has changed. Previously, in the Phase I report, a 10 percent efficiency factor for saline aquifers was applied. The current efficiency factors are 1 percent and 4 percent, which represent the P15 and P85 probabilities. This reduction in efficiency factors results in a reduction in the reported MRCSP Phase I values by factors between 2.5 and 10.

The storage capacity calculations for the saline aquifers were conducted using GIS software, specifically the raster-based Spatial Analyst extension of the ArcGIS software system. The general procedure for performing the calculations is to first create a structure contour grid and an isopach grid for the saline aquifer sequestration unit (Venteris and others, 2005). The structure elevation grid is then subtracted from a surface digital elevation model (DEM) to obtain a depth grid. The reservoir pressure is obtained by multiplying the fresh water pressure gradient of 0.433 psia/ft (9,792.112 Pa/m) with the depth grid, which results in the formation fluid pressure at depth. To obtain the reservoir temperature, the geothermal gradient grid is multiplied by the depth and the surface temperature grid is added to this result. Using a custom created macro (modified from Radhakrishnan and others, 2004) to access the CO_2 density values in a database table, these new reservoir pressure and temperature grids are then used, along with the isopach grid and the average porosity for the sequestration unit, to calculate the CO_2-sequestration capacity.

Results/Discussion

The original calculations, methodology, and reservoir characteristics, are the same as the MRCSP Phase I report for the Rose Run unit of the Knox Dolomite Formation, Potsdam, Conasauga, and Rome trough formations, except the Phase II report includes additional data from the state of New York for the Rose Run and Potsdam. The Phase I storage capacity estimates, using 10 percent efficiency factors, for the Cambrian formations were 56,460 million metric tonnes (MMt) (Table AD1). Using the same Phase I calculations the storage capacity estimates with the updated standard storage efficiency of (P15) 1 percent and (P85) 4 percent results in values of 6,920 MMt and 27,696 MMt (Table AD 2). The main difference between Phase I and II is that data from the state of New York is added and updated storage efficiency factors are used. Based on these updated Phase II results, the storage capacity of these Cambrian formations is approximately 29 percent of the Mount Simon Sandstones capacity.

Figure 1 Regional Stratigraphy Correlation Chart

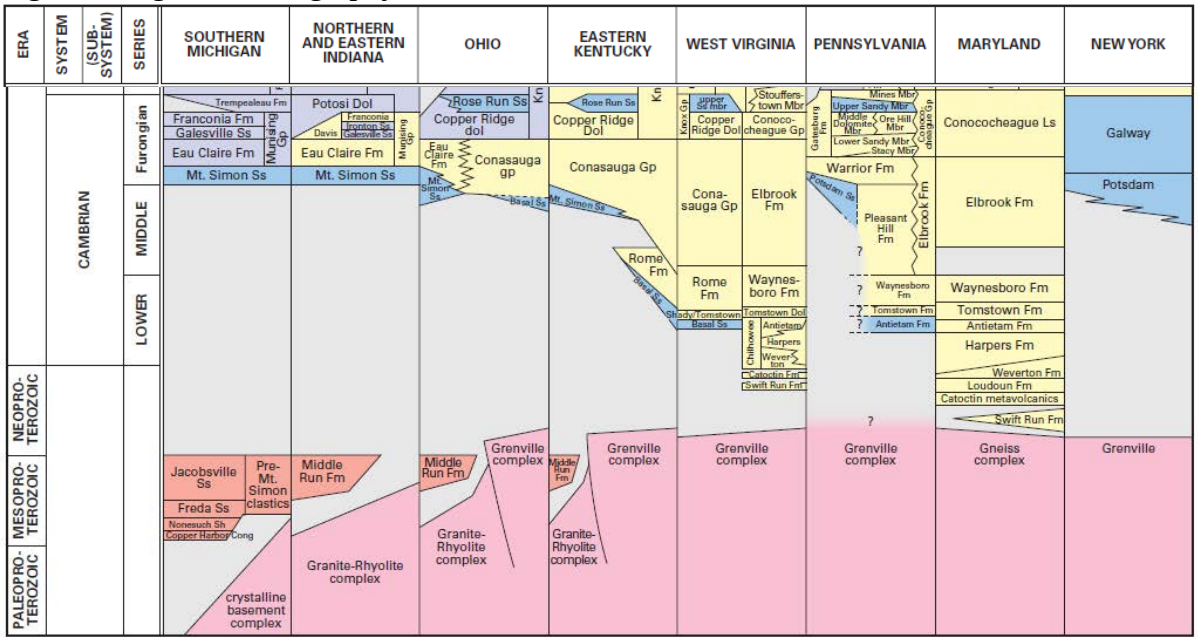

Table AD 1. Cambrian formation Phase I and Phase II storage capacity comparison.

Formation	Phase I (10%) (MMt)	Phase II (1%-4%) (MMt)
Rose Run	49,270	6,099 – 24,398
Potsdam	1,710	276 – 1,105
Conasauga Formation	4,250	426 – 1,702
Rome trough Sandstones	1,230	123 - 491
Total	**56,460**	**6,924 – 27,696**

Table AD 2. Cambrian formation storage capacity (MMt) (not including Mount Simon Sandstone)

Formation	Kentucky	Michigan	New York	Ohio	Pennsylvania	West Virginia	**Total 1% (MMt)**	**Total 4% (MMt)**
Rose Run	544 / 2,177	76 / 305	1,172 / 4,690	81 / 3,240	2,975 / 11,900	522 / 2,086	**6,099**	**24,398**
Potsdam			106 / 423		17 / 682		**276**	**1,105**
Conasauga Formation	0.15 / 0.593	16.4 / 65.7		347 / 1387	46 / 184	16.1 / 64.5	**426**	**1,702**
Rome Trough sandstones	100 / 400			0. 59 / .2.35		22 / 88.5	**123**	**491**
Total							**6,924**	**27,696**

References Cited

Capacity and Fairways Subgroup of the Geologic Working Group of the DOE Regional Carbon Sequestration Partnerships, 2007, Appendix A: Methodology for development of carbon sequestration capacity estimates, *in* Carbon sequestration atlas of the United States and Canada: U.S. Department of Energy, Office of Fossil Energy, National Energy Technology Laboratory, p. 71-86, http://www.netl.doe.gov/publications/carbon_seq/atlas/index.html

Radhakrishnan, P., Solano-Acosta, W., and Rupp, J.A., 2004, Sequestration of CO_2 in various geological media: An assessment of potential volumes in Indiana using GIS tools, *in* 2004 Eastern Section AAPG Meeting, October 3-5, 2004, Columbus, Ohio: AAPG Search and Discovery Article #90031, http://www.searchanddiscovery.com/documents/abstracts/2004eastern/radharkrishnan.htm, lasted accessed 6/10/2005.

Venteris, E.R., Solis, M.P., Carter, K.M., and McDonald, J., 2005, Uncertainty and grid-resolution analysis for regional-scale geologic maps, *in* IAMG Conference, Toronto, Canada, August 21-26: IAMG Conference Proceedings.